

TWELFTH EUROPEAN ROTORCRAFT FORUM

Paper No. 26

EXPERIMENTAL INVESTIGATION OF THE PERIODICAL
WAKE STRUCTURE OF A WIND TURBINE MODEL

L. Deppe, W.J. Wagner
DFVLR Institute of Aeroelasticity, Göttingen, F.R. Germany

September 22 - 25, 1986

Garmisch-Partenkirchen
Federal Republic of Germany

Deutsche Gesellschaft für Luft- und Raumfahrt e.V. (DGLR)
Godesberger Allee 70, D-5300 Bonn 2, F.R.G.

EXPERIMENTAL INVESTIGATION OF THE PERIODICAL WAKE STRUCTURE OF A WIND TURBINE MODEL

by

L. Deppe, W.J. Wagner
DFVLR Institute of Aeroelasticity,
Göttingen, F.R. Germany

Abstract

The spatial and time-dependent flow phenomena in the tip region of the wake of a wind turbine model were measured. For this reason the time-dependent running times of ultrasonic pulses transmitted through the flow were recorded by means of a testing device synchronized with the rotation of the wind turbine rotor. The translational velocity, path and the circulation of the tip vortex were determined for various operational states of the wind turbine. The velocity distribution in the rotor plane during a rotation is illustrated in a 3-D figure. This figure provides good insight into the fine structure of the flow phenomena in the immediate vicinity of the rotating blade.

Notation

ALPHA	pitch angle
c	velocity of sound
NROT	revolutions per minute
R	blade radius
RO, r_0	diameter of the vortex core
s	measuring path
t_w	running time of the ultrasonic pulse
$u_{(x)}$	velocity component of the flow field in sound direction
U_v	translational velocity of the vortex core
UAN, U_∞	freestream velocity
UMAX	maximum circumferential velocity of the vortex core
U_x	freestream velocity in the wake in main flow direction
x, x_k	coordinates
y, y_k	coordinates
Γ	circulation
λ	tip speed ratio (ωR)/(UAN)

1. Introduction

Within the scope of a cooperation project with the industrial firm M.A.N.-New Technology, Munich, the objective was established to obtain further measured data on a wind turbine model (GROWIAN rotor model). Particular attention was paid to the outer blade area, especially the blade tip. It is well known that this is the aerodynamically most effective area and is the most critical part of the wind turbine with respect to mechanical loads. The desire to make specific constructional changes, e.g. to improve performance, to reduce mechanical loads and to lessen the generation of noise which is significantly influenced by the tip region, requires reliable detailed knowledge of the flow phenomena. The published literature on this topic chiefly provides measured data of rotor systems in the form of mean values; there is a definite need for values in the time

domain. For these reasons we planned to investigate the spatial and time-dependent flow field in the wake of the blade tips.

The performance of this project was made possible by the availability of an ultrasonic measuring system for investigating unsteady flow phenomena. This system, developed in the DEVLAR Institute of Aeroelasticity [1], is an extension of the steady method by D.W. Schmidt [2]. Since the facility had previously been used for nonrotating systems [3], it was necessary to modify it in the present experiment for use in a rotating system.

The global program can be broken down into the following points:

- a) Measurement of the tip vortex parameters and the behavior of the vortex in the rotor wake.
- b) Measurement of the periodical flow field velocity in the rotor plane and extended planes in the wake.
- c) Calculation of the radial lift distribution on the blade using the ultrasonic anemometry results.
- d) Influence of specific changes of the blade tip shape on the events stated in a) through c), with simultaneous measurement of the mechanical values.
- e) Use of a tip vane configuration as a special tip shape.

The program is presently in the beginning phase: points a) and b) have been performed in a windtunnel experiment; W. Send [4] has developed approaches to solve point c). Points d) and e) are intended for the next phase of the program. Preliminary results for points a) and b) are presented in this paper. The evaluation is not yet complete.

2. Description of the test setup

2.1 The wind turbine model and its windtunnel setup

The photograph in Figure 1 shows the wind turbine model setup in the settling chamber of the 3 m x 3 m Low-Speed Windtunnel in Göttingen. The settling chamber of 7 m x 7 m diameter was chosen for the test section because the turbine with its diameter of 4 m could not have been accommodated in the main test section and because velocities up to approximately 12 m/s can be

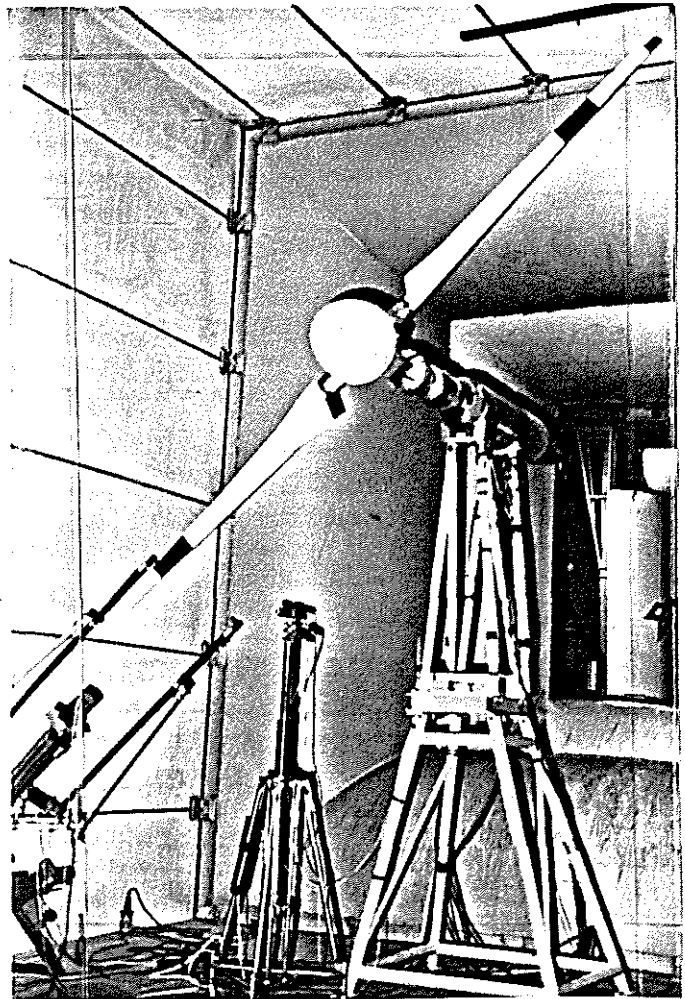


Figure 1 Wind turbine model in the settling chamber of the windtunnel

reached. This value corresponds to the rated wind velocity of GROWIAN. The ultrasonic test section mounted on a slide table can be seen in the lower left corner. To the left of the tower there is a laser optical system on a tripod for recording a preset rotational angle of the rotor blades.

The fundamental mechanical measurements were performed in 1981 on the same wind turbine test setup by G. Pearson [5] of M.A.N.-New Technology in collaboration with DFVLR Göttingen. With respect to rotor blade length, hub radius and blade chord distribution, the wind turbine is a 1 : 25 scale model of GROWIAN, hence it has a diameter of 4 m. A Clark profile is used in the outer region and a GÖ 625 in the inner region, deviating from the the original Wortmann FX 7W profiles in order to simulate analogous lift and drag behavior at a smaller Reynolds number. The nacelle and the tower construction are part of a modified propeller test setup provided by the DFVLR Division of Low-Speed Windtunnels. With this test setup, it is possible to supply the rotor shaft with up to approximately 65 kW at a controlled rotational rate or to withdraw power generation. The entire C_p - λ field can be covered by varying the rotational rate and/or flow velocity. The forces and moments acting on the wind turbine are measured by a 6-component strain gauge balance and the power output is calculated by a computer program.

Strain gauges are installed on both blade roots to measure the root bending moments; the signals are transmitted from the rotating system via a co-rotating preamplifier and slip rings.

2.2 Ultrasonic measuring principles

The fundamental ultrasonic measuring principles are shown in Figure 2. The flow field of interest is located between an ultrasonic transmitter and receiver. At a prescribed instant, the transmitter emits a short sonic pulse which travels at the speed of sound toward the receiver, where it is picked up a moment later. The local running velocity of the sonic pulse as it crosses the flow field equals the vector sum of the speed of sound and the velocity field. The running time of the ultrasonic pulse which results from the summation along the sonic path is measured. The measured running time is hence the integral:

$$t_w = \int_0^s \frac{dx}{c - u(x)}$$

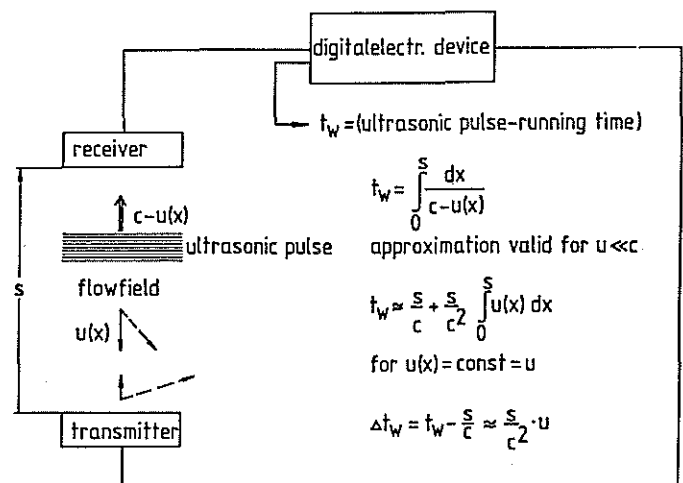


Figure 2 Principles of ultrasonic measuring and the relation between running time and flow field. The measured running time is hence

By means of a Taylor expansion which is stopped after the second term, we obtain for $u \ll c$ an approximation formula for the correlation between running time and velocity:

$$t_w \approx \frac{s}{c} + \frac{s}{c^2} \int_0^s u(x) dx$$

for $u(x) = \text{const.} = u$

$$\Delta t_w \approx t_w - \frac{s}{c} \approx \frac{s}{c^2} \cdot u$$

Thus it can be seen that the measured running time and velocity are approximately proportional.

Since the measurements are taken with the conditional sampling method, which requires that an exact relationship to the momentary angle of rotation be maintained, a time pulse synchronized with the angle is generated by an optoelectronic position detector equipped with a laser lighting system. This pulse is fed into the trigger input of the LPS system of the PDP 11/34 computer. With the additional knowledge of rotation frequency and a given division of the phase, the computer calculates the moment at which a cycle of one ultrasonic measurement should begin. At this moment a pulse is transferred from the analogue output of the computer to the trigger input of the circulation measuring setup, and this pulse starts the ultrasonic pulses of the measuring and the reference beams. A short time (10 μ s) before the expected arrival of the reference ultrasonic pulse at the receiving microphone, the counter is reset by means of a pulse which is delivered by the digital output. Upon arrival of the reference pulse, the counter will be started; arrival of the measuring pulse stops the counter. This stopping pulse is fed into the data-ready line of the computer and will cause the computer to accept from the counter the measured time value as BCD-coded data. This small cycle is repeated a prescribed number of times (in this case we chose 50 times). A new sweep pulse of the blade repeats the big cycle.

The flow chart of the process control and data acquisition is shown in Figure 3. Because of the high speed required, the corresponding program is written in machine language. Effort must go into avoiding and rejecting numerous possible errors without sacrificing synchronization with the rotor revolutions. The computer will check whether the accepted time-measuring values lie within a prescribed interval. If one of them does not, it will be rejected and a message appears on the monitor. The accepted values are stored on the disk for further calculations and are simultaneously used to obtain a mean value for every phase interval. The development of these mean values

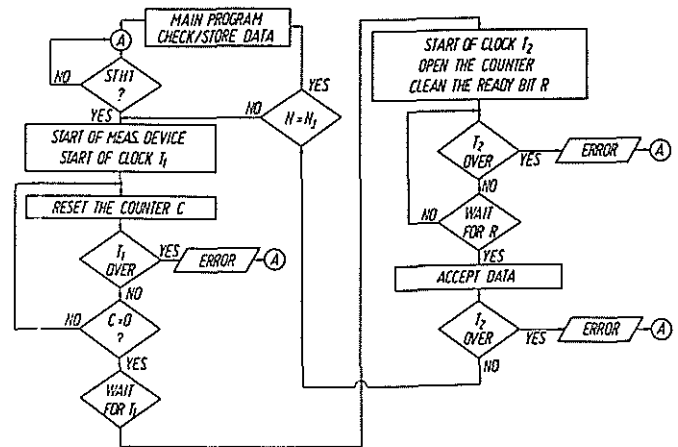


Figure 3 Schematic diagram of test setup for processing and acquisition of data

(variation of Δt_w with phase) is displayed on the monitor in real time.

The quality of the measurements proved good enough to allow individual measurements to be used as direct results. During this experiment we fixed the sample rate for measurements at 500 per second, so that we obtained a time resolution of 2 ms on the running time signal output.

Figure 4 is a block diagram of the entire test setup for measuring ultrasonic running times in the flow field of the test rotor. It comprises first of all a linear arrangement of two ultrasonic microphones (a transmitter and a receiver) located opposite each other at a distance of approximately 50 cm which is fixed by a rigid mechanical support

of 150 cm shaft length. This support, a custom CFK tube construction, is attached to a slide table driven by stepping motors. The microphone system may thus be moved in the main flow and in radial direction. The rigid support is constructed such that it can be shifted radially over the rotating blade. The direction of the sonic beam can be independently adjusted in all directions. A special feature of this test method is that the flow field of interest remains largely undisturbed by the measuring devices (microphones).

The spatial conditions and the wake structures of the wind turbine are shown in Figure 5. In the schematic sketch the tip vortices, generated by the two blade tips, can be seen drifting at a velocity of U_v in a spiral fashion into the wake.

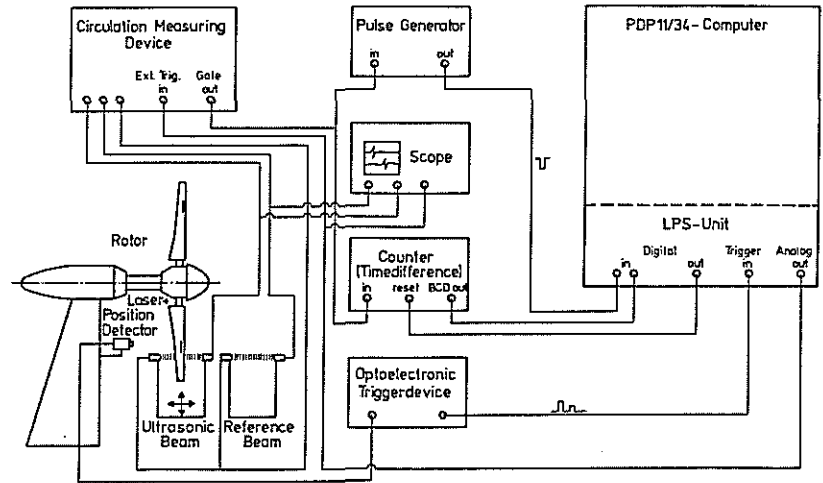


Figure 4 Flow diagram of the data acquisition procedure

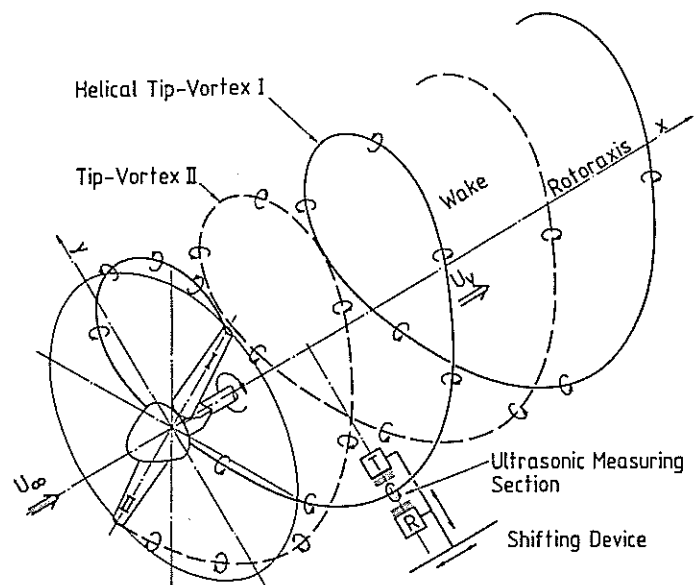


Figure 5 Schematic view of the wind turbine, its wake and the positioning of the ultrasonic measuring device

The ultrasonic measuring device with its test section in radial position is arranged such that the vortex axis crosses the sonic beam vertically at a velocity of U_y . In this manner the integrated velocity profile of the vortex is pictured as a running time signal.

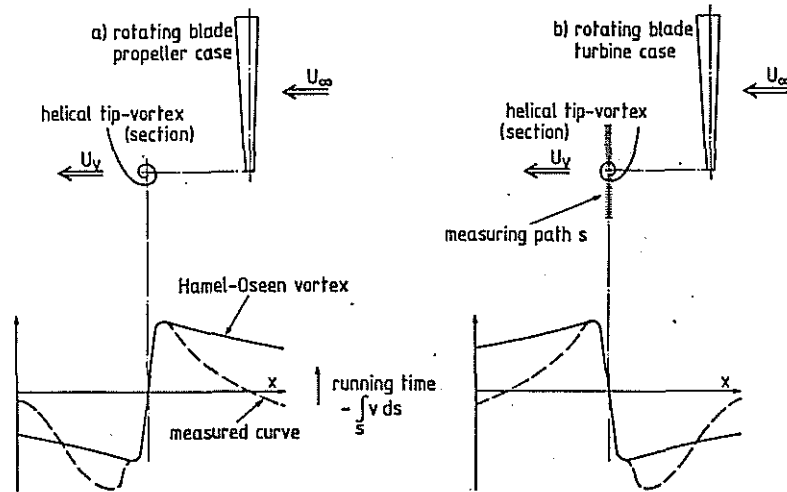


Figure 6 The helical tip vortices of a wind turbine recorded by the ultrasonic measuring device
a) Energy consumption b) Energy production

The two polar cases for the tip vortices in the wake are pictured in Figure 6; Fig.6a shows the case in which the turbine operates as a propeller, thus releasing energy into the flow and accelerating the wake; Fig.6b shows the turbine operation where energy is extracted from the flow. In the former case the vortex rotates counterclockwise, in the latter case it rotates in clockwise direction. The diagrams beneath the figures represent the corresponding running times as they are registered when the vortex passes through the test section. Hamel-Oseen vortices are provided as a theoretical model, which however describe the flow phenomena only within a limited radius area about the vortex core. The deviations occurring farther outside this area will be discussed below based on test results.

A Hamel-Oseen vortex expressed as running time versus location is pictured in Figure 7. The vortex is mathematically determined by the following four parameters:

1. y-coordinate of the vortex center,
2. Δt_w -value of the vortex center,
3. diameter of the vortex core r_0 ,
4. maximum circumferential velocity u_{max} .

These parameters were used to evaluate the test results to be discussed below.

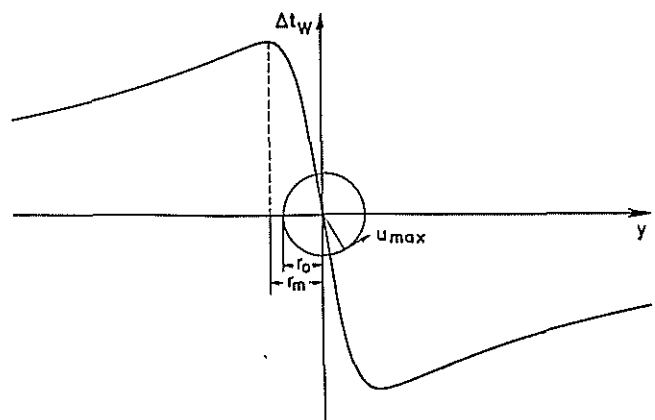


Figure 7 Hamel-Oseen vortex recorded by the ultrasonic measuring device

3. The helical tip vortices in the wake

The test results obtained with the arrangement of the test section shown in Fig.5 are presented in Figure 8. The test section is located in axial position 95 cm downstream of the rotor. The running time recorded at intervals of 2 ms is represented by the vertical axis versus time on the horizontal axis. The steep jump in the curves signals the passage of the tip vortex core through the test section. Each diagram pictures an individual vortex as it crosses the test section during a blade revolution. One can see that the curve shapes are qualitatively quite similar, although a certain stochastic scattering is evident. This scattering is caused by the oscillations of the rotor blades and the turbulence of the flow; a certain role is also played by the limited resolution of the measuring system. In general, however, it can be clearly recognized that the time-dependent formation as well as the structure of the vortex are quite stable.

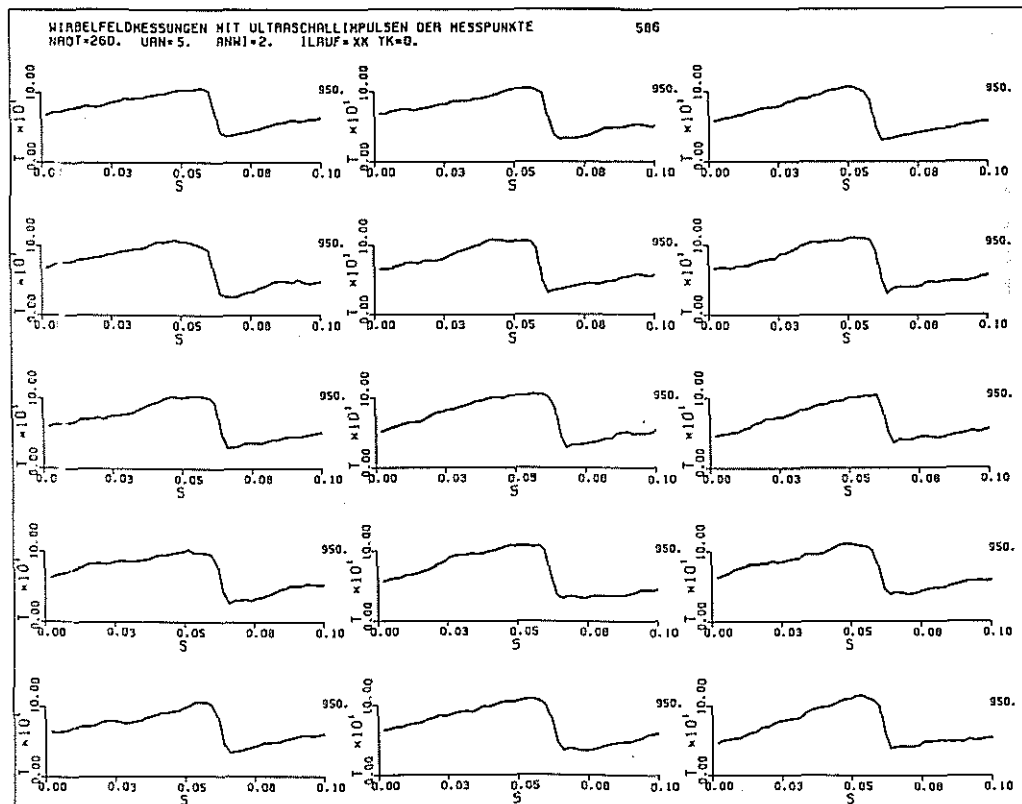


Figure 8 Series of individual successive vortices measured at a downstream position $x_k = 95$ cm

Figure 9 shows an entire sequence of curves recorded at various positions in downstream direction. The initial position is at $x_k = 10$ cm, the final position at $x_k = 95$ cm downstream of the rotor plane. The smoother curves are due to the fact that mean values of over 50 measurements make up each curve. The displacement of the steep transitions from diagram to diagram of the curve sequence clearly indicates the translational movement of the recorded tip vortices. Information on the translational velocity of the tip vortices is contained in these displacements. One can also clearly see the changing curve shapes, which is particularly distinct in the area directly behind the rotor plane.

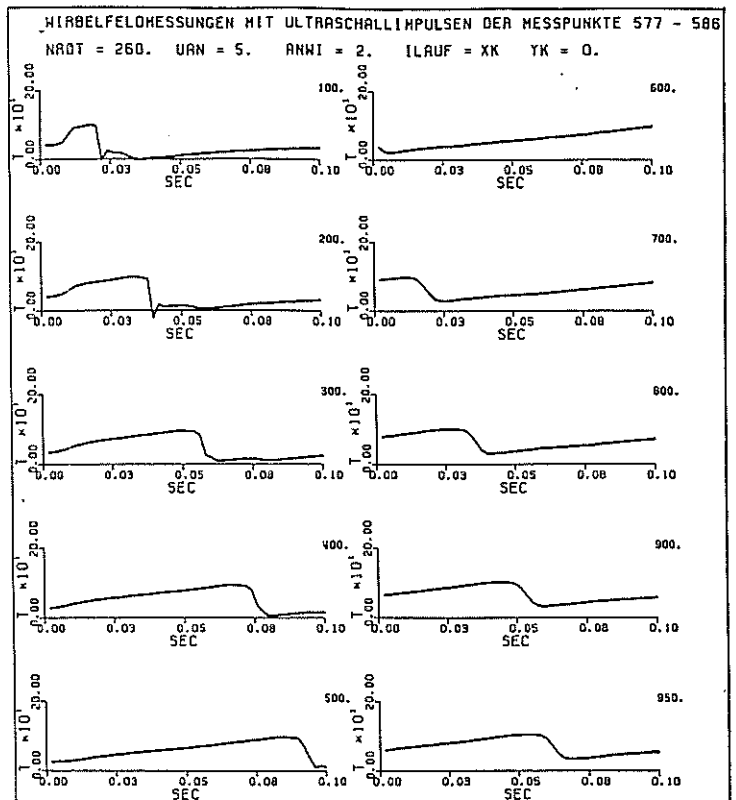


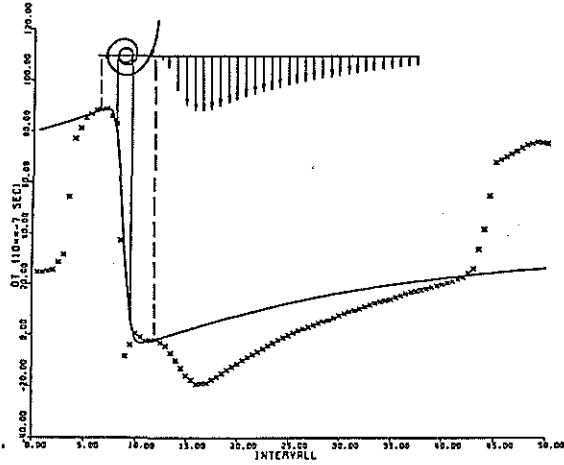
Figure 9 Variations of curve shape with increasing downstream position

The specific curve shape and the related physical flow phenomena shall now be discussed with reference to the example given in Figure 10. For the positions 10, 20, 30, 40 and 50 cm downstream of the rotor plane, the points of the mean running time curves are represented by crosses. The solid lines correspond to theoretically calculated curves based on the Hamel-Oseen vortex given above. These curves have been fitted to the measured curves by means of a computer-aided procedure. The corresponding vortex parameters are listed above. The curve fit was performed such that primarily the vortex core region of the theoretical curve was brought into exact agreement with the steep transition of the measured curve; as a further criterion the step height of the theoretical curve was fitted to that of the measured curve. The satisfactory agreement for the vortex core and its immediate vicinity thus achieved can be clearly seen. This means that theoretical calculations deliver good values for the location of the vortex core and circulation. The deviations become greater with increasing distance from the vortex core. The Hamel-Oseen vortex approach surely does not describe the entire flow phenomenon here, but it fits in with the following hypothetical statements:

- a) The flow immediately behind the rotor blades is determined by the energy output on the blades. This means a delay in axial direction. For continuity reasons, a radial expansion of the flow takes place.
- b) This process occurs in the flow behind the blade; it circulates therefore with the blade and is thus a periodical process with respect to fixed spatial coordinates.

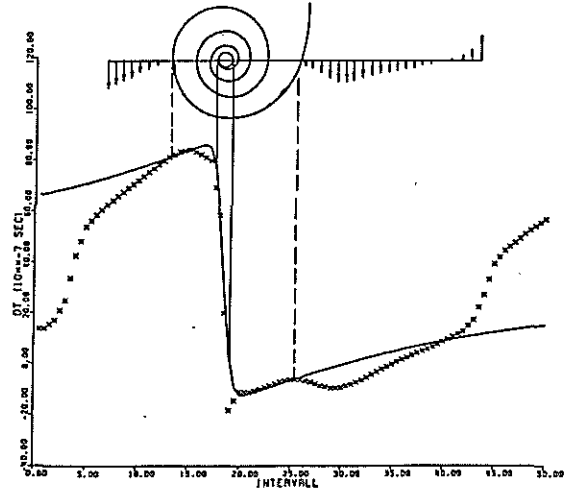
WIRBELANPASSUNG DES MESSPUNKTES 576

NRDT (U/MIN) = 360. UAN (M/S) = 5. XK (MM) = 100.
 ALPHA (GRAD) = 2. FREQ (HZ) = 10. YK (MM) = 0.
 R = 1.99 RO (CM) = 0.86 UHAX (CM/S) = 1291.79
 YRA (CM) = 8.76 DTWD (MS) = 42.16



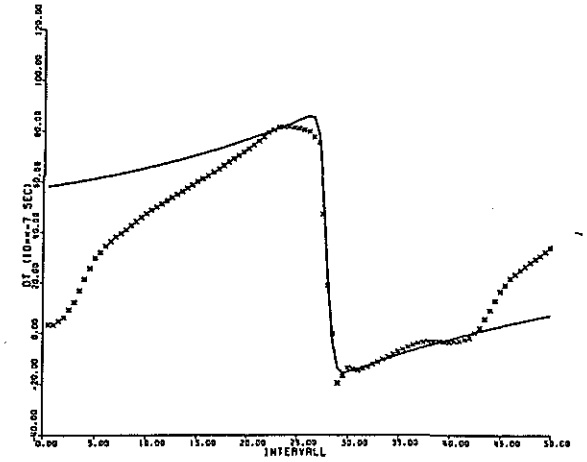
WIRBELANPASSUNG DES MESSPUNKTES 575

NRDT (U/MIN) = 360. UAN (M/S) = 5. XK (MM) = 200.
 ALPHA (GRAD) = 2. FREQ (HZ) = 10. YK (MM) = 0.
 R = 1.69 RO (CM) = 1.07 UHAX (CM/S) = 1245.80
 YRA (CM) = 18.36 DTWD (MS) = 36.11



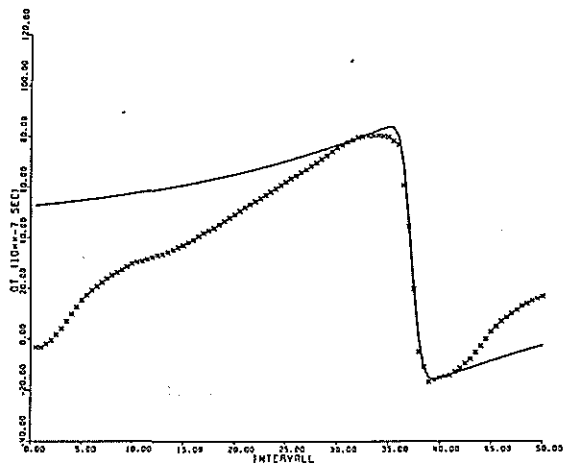
WIRBELANPASSUNG DES MESSPUNKTES 574

NRDT (U/MIN) = 360. UAN (M/S) = 5. XK (MM) = 300.
 ALPHA (GRAD) = 2. FREQ (HZ) = 10. YK (MM) = 0.
 R = 1.07 RO (CM) = 0.95 UHAX (CM/S) = 1423.47
 YRA (CM) = 27.82 DTWD (MS) = 34.33



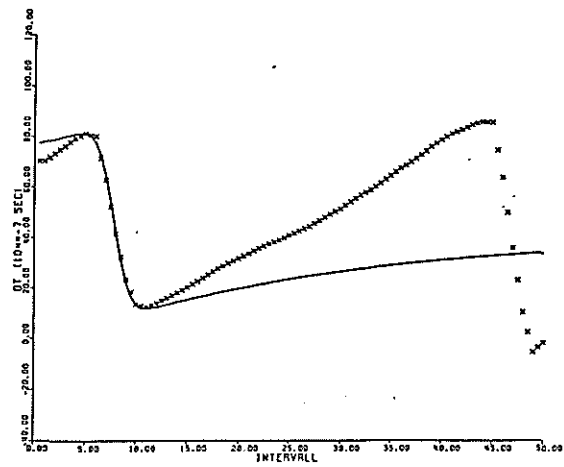
WIRBELANPASSUNG DES MESSPUNKTES 573

NRDT (U/MIN) = 360. UAN (M/S) = 5. XK (MM) = 400.
 ALPHA (GRAD) = 2. FREQ (HZ) = 10. YK (MM) = 0.
 R = 1.55 RO (CM) = 1.23 UHAX (CM/S) = 1103.53
 YRA (CM) = 37.26 DTWD (MS) = 33.70



WIRBELANPASSUNG DES MESSPUNKTES 572

NRDT (U/MIN) = 360. UAN (M/S) = 5. XK (MM) = 500.
 ALPHA (GRAD) = 2. FREQ (HZ) = 10. YK (MM) = 0.
 R = 0.84 RO (CM) = 1.95 UHAX (CM/S) = 500.00
 YRA (CM) = 7.83 DTWD (MS) = 46.45



WIRBELANPASSUNG DES MESSPUNKTES 571

NRDT (U/MIN) = 360. UAN (M/S) = 5. XK (MM) = 500.
 ALPHA (GRAD) = 2. FREQ (HZ) = 10. YK (MM) = 0.
 R = 1.39 RO (CM) = 1.80 UHAX (CM/S) = 697.94
 YRA (CM) = 47.01 DTWD (MS) = 40.65

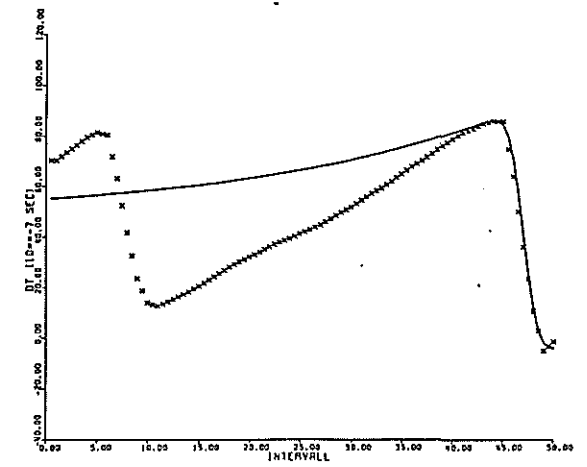


Figure 10 Running time curves fitted by means of a Hamel-Oseen vortex

- c) With respect to the (from a spatially-fixed point of view) likewise periodical tip vortex, the radial expansion occurs immediately behind the vortex.

Use of these statements to interpret the pictured curves yields a flow figure like the schematic view above the first diagram: the vortex moving to the left is followed by the radial flow expansion, which gradually fades until the next vortex passes.

The second diagram presents the situation 10 cm farther downstream: the central Hamel-Oseen vortex is further developed and its potential flow field is extended; the flow expansion is considerably weakened and has drifted to the right.

In the third diagram it can be seen that the flow expansion has faded at a distance of 30 cm from the rotor plane; the potential part of the vortex has expanded to the right whereas this is no longer the case on the left.

In the fourth, fifth and sixth diagrams at 40/50 cm in the wake, one finds a state characterized by two adjacent vortices and their interaction. The resulting radial flow field between them fades more quickly than predicted by the vortex potential law of a single vortex. Farther downstream, no substantial changes of the curve shapes take place, therefore precluding the need for an additional diagram; a relatively stable state has apparently been reached. It should also be mentioned in context with diagrams 5 and 6 that the two discernible vortices have significantly different circulations. This indicates that the two rotor blades are considerably different with respect to their flow characteristics.

Figure 11 shows as an example the case in which the turbine is operating as a propeller, i.e. it releases energy into the flow. As expected, the vortex has an opposite sense of rotation, which can be seen in the reversed curve. Notable in this context is again the difference between the circulations of the two successive vortices. Since the difference in this case is about a factor of 2, this phenomenon can no longer be explained by shape differences or inaccurately adjusted incidences of the two blades; rather, it must be assumed that the flow on one blade is still attached but is separated on the second blade, the result of which is the breakdown of lift and thus of circulation.

The following four figures show the translational velocity and circulation of the tip vortices in the wake for various states of operation of the wind turbine. These values were obtained by means of the vortex fitting procedure described above.

NROT (U/MIN) = 460. URN (M/S) = 5. XK (MM) = 900.
 ALPHA (GRAD) = 10. FREQ (HZ) = 10. YK (MM) = 0.
 A = 0.65 RD (CM) = 1.40 UNAX (CM/S) = -286.77
 YWA (CM) = 14.46 DTWO (MS) = 49.25

NROT (U/MIN) = 460. URN (M/S) = 5. XK (MM) = 900.
 ALPHA (GRAD) = 10. FREQ (HZ) = 10. YK (MM) = 0.
 A = 7.16 RD (CM) = 1.64 UNAX (CM/S) = -150.61
 YWA (CM) = 45.65 DTWO (MS) = 49.73

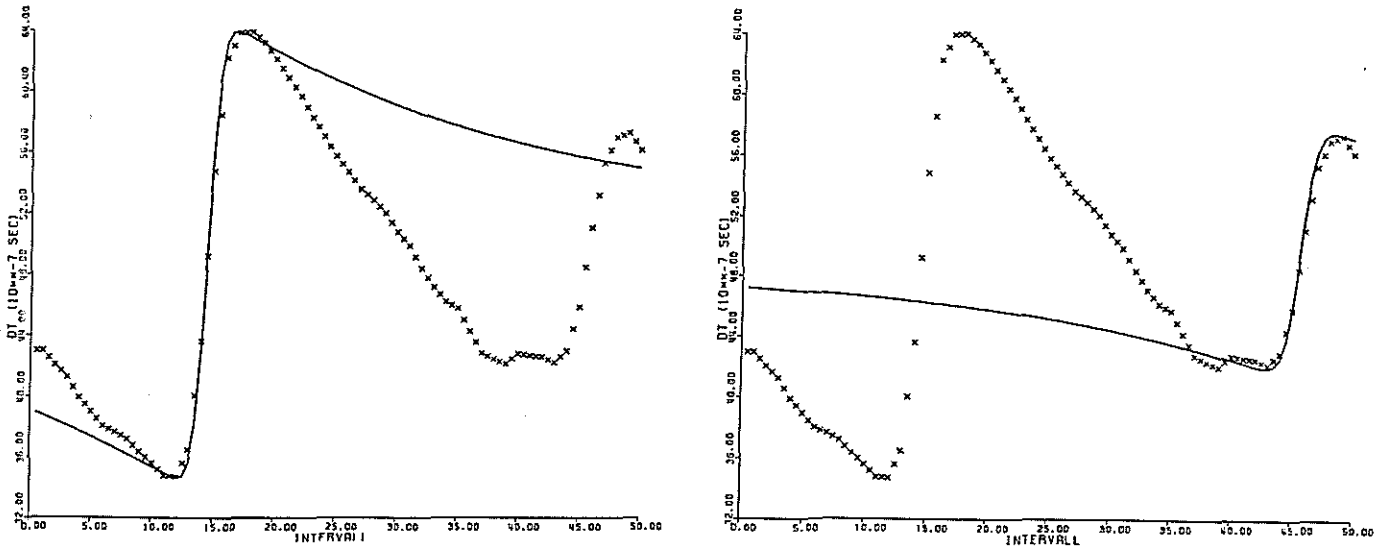
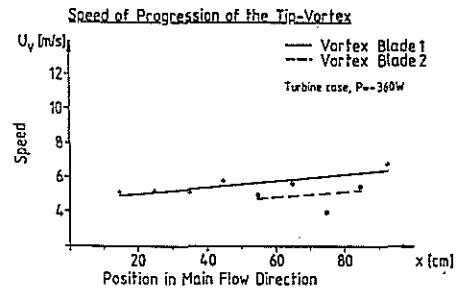
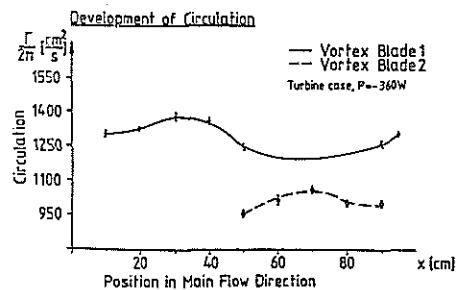


Figure 11 Running time curves with changed sense of vortex rotation in the case of propeller operation.

In Figure 12 the following conditions are valid: rotation frequency 360 1/min, freestream velocity 5 m/s, blade incidence 2° . The translational velocity begins at about 5 m/s and increases downstream until the position $x = 90$ cm to about 6 m/s, which is greater than the freestream velocity. In this context it must be mentioned that the wind turbine is located in a closed windtunnel shortly in front of the contracting intake region of the jet. Taking this into consideration, a delay of the axial velocity in the turbine wake indicates, for continuity reasons, an increase of the velocity between wake and wind-tunnel wall. The locations of the tip vortices define the transition region between the wake and the outer flow. Its translational velocity equals the mean velocity at the path of the vortex centers. The development of circulation is shown in the lower part of the figure. Directly behind the rotor plane, the circulation increases and then remains with minor fluctuations roughly at the same value. This behavior agrees with the initial increase of the circulation behind a nonrotating wing. The growth of the vortex circulation is due to the fact that the vortex increasingly rolls the flat vortex sheet of the wing about itself, thus causing a



Parameters: NROT = 360 1/min, $U_\infty = 5$ m/s, $\lambda = 15$, $\alpha = 2^\circ$



Parameters: NROT = 360 1/min, $U_\infty = 5$ m/s, $\lambda = 15$, $\alpha = 2^\circ$

Figure 12 Speed of progression and development of circulation of the tip vortex in the wake

concave curvature of the vortex axis with increasing downstream distance from the wing. In the case that the circulation within the rotating system remains constant, this also means that the vortex paths are straight parallels, as will be shown below. The dotted curves show, as discussed above, that the tip vortex of the second rotor blade has a smaller circulation as well as a reduced velocity. This behavior naturally produces a considerable asymmetry in the wake.

In Figure 13, the freestream velocity has been doubled to 10 m/s, while the other conditions remain the same. Qualitatively, the figure has not changed. The translational velocity is now at about 11 m/s, the circulation has approximately doubled, the turbine power output is approximately four times greater. The increase of circulation extends farther downstream although normalization to the "vortex age" would yield an agreement of the curves.

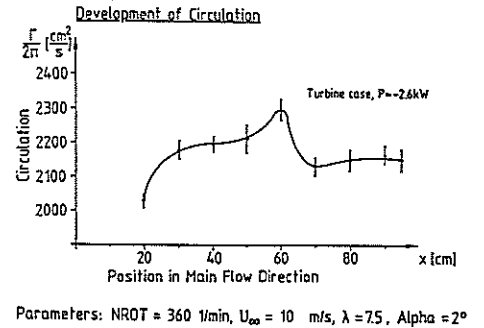
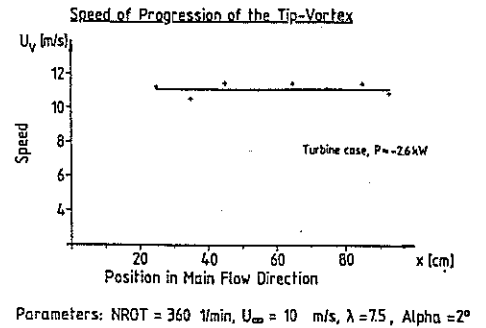
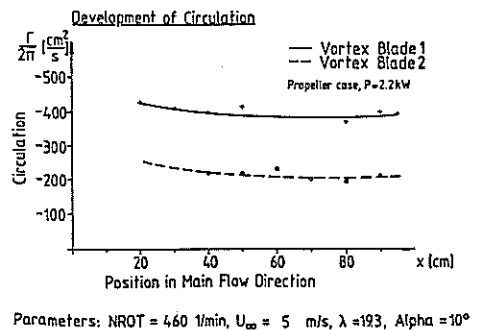
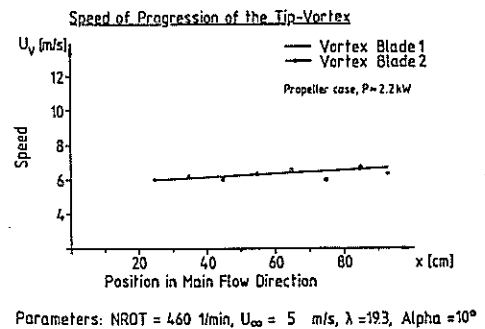
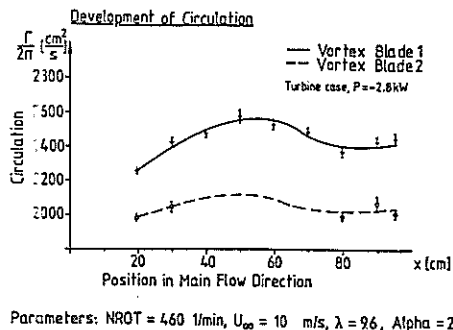
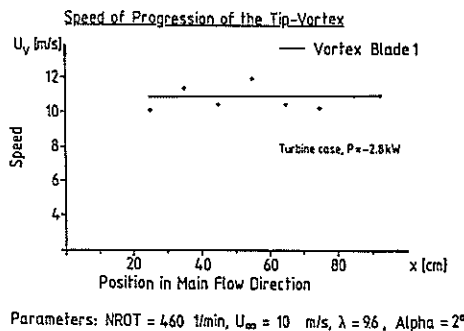


Figure 13 Speed of progression and development of circulation of the tip vortex in the wake



Figures 14 and 15 Speed of progression and development of circulation of the tip vortex in the wake

In Figure 14, the rotational frequency was raised to 460 1/min. Since this case no longer falls so ideally within the field of power coefficient curves, the power output is barely raised, the translational velocity and the circulation are almost identical with the previous figure.

Finally, Figure 15 shows the conditions of the case demonstrated above of the wind turbine operating as a propeller. Notable here is the translational velocity which increases from 6 m/s to 7 m/s and thus reflects the acceleration of the rotor wake.

Figure 16 shows for one operational state of the turbine the radial path of the tip vortex centers in the rotor wake. One can see that the path follows a straight line, which means that, as mentioned above, no further rolling process of the vortex takes place. Lastly, Figure 17 is a three-dimensional illustration of the axial velocity field in the rotor plane with the blade in rotation. This velocity field was also obtained by means of the ultrasonic measuring device, with the sonic pulses crossing the rotor plane. The skips in the lines indicate the places where the rotating blade blocked the measurement, i.e. the emitted sonic pulse was kept from reaching the receiving microphone. This figure constitutes a concentrated illustration of much information; It is helpful to imagine the perspective of Fig.17 as if one were looking into a stadium. Particularly interesting is the region immediately before and after the blade crossing. The energy output at the blade is seen as a sudden velocity reduction which quickly fades in the broader surrounding area. The velocity increases from the inner to the outer measuring radius by about 30%. The greatest velocity jumps and gradients occur in the area where the tip vortices develop; this is obviously the region which is enormously significant for energy conversion.

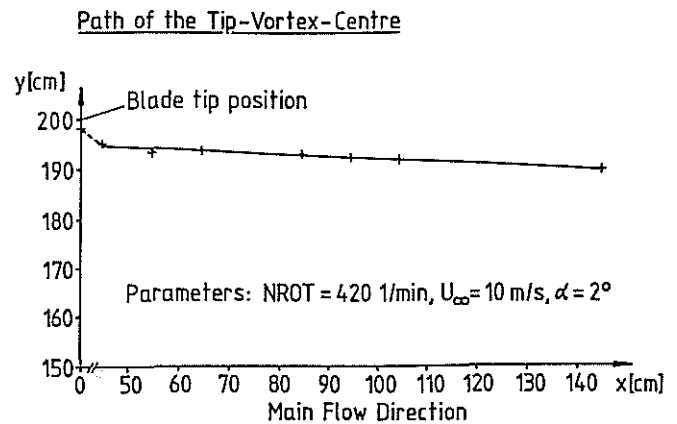


Figure 16 Path of the tip vortex center in the wake

4. Conclusions

- a) The measurements performed in a reasonable amount of time in a rotating system using the ultrasonic device introduced here shed light on the spatial time-dependent structure of the rotor wake.
- b) The translational velocity, path and development of circulation of the helical tip vortex can be determined for certain states of operation; definite relationships were found for each state of operation.
- c) The diagram of the measured flow field in the rotor plane clearly illustrates the physical phenomenon at the rotating blade. This could prove to be a useful aid for the design of rotors, especially the tip region.

5. References

- [1] Engler, R.H. Experimental Study of Tip Vortices behind
Wagner, W.J. an Oscillating Blade by the Ultra-Sonic
Weitemeier, B. Method.
Proc. Colloq. honoring H.G.Küssner on 80th
birthday, Göttingen (1980) pp.119-129.
- [2] Schmidt, D.W. Acoustical Method for Fast Detection and
Measurement of Vortices in Wind Tunnels.
ICIASF '75 Record (1975) pp.216-228.
- [3] Wagner, W.J. Comparative Measurements of the Unsteady
Pressures and the Tip-Vortex Parameters on
Four Oscillating Wing-Tip Models.
Proc. Symp. on Unsteady Aerodynamics of Tur-
bomachines and Propellers (1984) Cambridge,
UK.
- [4] Send, W. The Prediction of Lift Distribution Inferred
from Downstream Vorticity Measurements.
Proc. 15th ICAS Congress (1986) London, UK.
- [5] Pearson, G. Windtunnel Measurements on a 1/25th Scale
Model of the GROWIAN Rotor.
Part I: Model Design, Construction and Per-
formance Measurements on a Rigid Rotor with
Symmetrical Flow.
Internal M.A.N. Report (1981).